UNIVERSITÀ DEGLI STUDI DI TORINO

Phosphate glass fibres and their role in neuronal polarization and axonal growth direction

C. Vitale-Brovarone [a,⇑], G. Novajra [a], J. Lousteau [a], D. Milanese [a], S. Raimondo [b], M. Fornaro [b, c]

[a] Materials Science and Chemical Engineering Department, Politecnico di Torino, Corso Duca degli Abruzzi 24, 10129 Torino, Italy
[b] Neuroscience Institute ‘‘Cavalieri Ottolenghi’’ & Department of Clinical and Biological Sciences, University of Turin, Regione Gonzole 10, 10043 Orbassano, Italy [c] Department of Anatomy, Midwestern University, 555 31st Street Downers Grove, IL 60515, USA

A b s t r a c t

Phosphate glass fibres with composition 50P2O5–30CaO–9Na2O–3SiO2–3MgO–(5 _ x)K2O–xTiO2 mol.% (x = 0, 2.5, 5, respectively coded as TiPS0, TiPS2.5 and TiPS5) were drawn following the preform drawing approach. A 20-day solubility test in bi-distilled water was carried out on glass fibres with different compositions and diameters ranging between 25 and 82 lm. The results show that the glass composition, the initial fibre diameter and the thermal treatment are the main factors influencing the dissolution kinetics and that the fibres maintain their structural integrity and composition during dissolution.

Biological tests were carried out on aligned TiPS2.5 glass fibres using Neonatal Olfactory Bulb Ensheathing Cell Line (NOBEC) and Dorsal Root Ganglia (DRG) neurons. The fibres showed to be permissive substrates for cell adhesion and proliferation. The aligned configuration of the fibres seemed to provide a directional cue for growing axons of DRG neurons, which showed to sprout and grow long neurites along the fibre axis direction.

These promising findings encourages further studies to evaluate the potential use of resorbable glass fibres (e.g. in combination with a nerve guidance tube) for the enhancement of the peripheral nerve healing with the role of supporting and guiding the cells involved in the nerve regeneration.

1. Introduction

Phosphate glasses present the advantage of being completely soluble in aqueous media with a dissolution rate that can be tai-lored by varying the glass composition in order to match the de-sired resorption time [1,2]. The solubility of phosphate glasses and the possibility of producing them in bulk, powder, porous scaf-fold or flexible fibre forms make them suitable for the design of resorbable biomedical devices for both hard and soft tissue regen-eration [3]. These glasses have been studied for bone tissue regen-eration in powder and porous scaffold forms or in composite materials [4–9], for application in the hard–soft tissue interface such as the ligament–tendon/bone attachment defects [10–12]. In addition, resorbable and flexible phosphate glass fibres are attractive materials for soft tissue regeneration. Ahmed et al. [13] observed cell attachment and differentiation of conditionally immortal muscle precursor cells on phosphate glass fibres, with the formation of myotubes along the axis of the fibres. Shah et al. [14] investigated the use of phosphate glass fibres as a poten-tial scaffold material for the in vitro engineering of craniofacial skeletal muscle. They found that a three-dimensional mesh of fi-bres enhanced the attachment and proliferation of human masse-ter-derived cells, which were also capable of migrating along the fibres.

In this work, phosphate glass fibres are studied for their poten-tial application in the treatment of peripheral nerve injuries, with the role of supporting and guiding the cells involved in the nerve regeneration. Previous results from Bunting et al. [15] showed that fibres of silicate glass (Bioglass 45S5) support Schwann cell and fibroblast growth in vitro and axonal regeneration in vivo when placed within a silastic tube for the treatment of peripheral nerve damage.

Peripheral nerve injuries, resulting from trauma or disease, can lead to partial or total loss of motor,

sensory and autonomic func-tions in the area of the body concerned. Following axonal disrup-tion, regeneration occurs by the sprouting of new daughter axons from the proximal stump, forming a ''regenerating unit'' sur-rounded by a common basal lamina [16]. Wallerian degeneration of the axons occurs in the distal stump, in which Schwann cells and infiltrating macrophages participate in clearing axonal, myelin and tissue debris; Schwann cells proliferate and become aligned within the endoneurial tubes, forming the bands of Büngner, which guide regenerating axons along the distal stump [16].

For severe injuries, recovery is unlikely to occur without surgi-cal intervention. For short nerve gaps, end-to-end suturing is car-ried out, in which the two nerve stumps are sutured, while for nerve gaps longer than 2 cm, the current gold standard is the use of an autologous nerve graft [17,18]. However, the harvesting of nerve tissue from the patient implies obvious drawbacks and, in addition, use of an autograft may show insufficient length and diameter for reconstruction. For these reasons, nerve guidance channels based on polymeric materials sutured in-between the two nerve stumps have been developed and are currently used to assist in directing axons from the proximal to the distal nerve stump [19,20]. At present, the use of such guidance channels is limited to short nerve defects, up to 3 cm [21]. For large nerve gaps, exogenous supports are needed to enable the regenerating fibres to cross the gap [18]. In this context, the use of growth permissive mi-cro- or nanofibres could be a possible strategy.

In a previous work, a series of phosphate glasses, coded TiPS, were developed (50P2O5–30CaO–9Na2O–3SiO2–3MgO–(5 _ x) K2O–xTiO2 mol.%, x = 0, 2.5, 5) and showed different dissolution rates, good biocompatibility with MG-63 osteoblasts and suitable characteristics for being drawn into fibres with micrometric diam-eters [22,23]. In this study, TiPS glasses were characterized in term of viscosity features and were drawn into fibres. A dissolution test was carried out in order to study the factors influencing the fibre dissolution rate, such as glass composition, fibre diameter and thermal treatment. Finally, biological tests were carried out in or-der to investigate the interaction between fibres and either neona-tal olfactory bulb ensheathing cell (NOBEC), a type of glial cell [24], or dorsal root ganglia (DRG) dissociated neurons.

2. Materials and methods

2.1. Glass preparation

Three phosphate glasses with composition (mol.%) 50P_2O_5– 30CaO–9Na_2O–3SiO_2–3MgO–(5 _ x)K_2O–xTiO_2, with x equal to 0 ($TiPS_0$), 2.5 ($TiPS_{2.5}$) and 5 ($TiPS_5$), were prepared through the melt-ing and quenching technique. The precursors, P_2O_5 (purity 99.9%), $Ca_3(PO_4)_2$ (purity 96%), NaH_2PO_4 (purity 99.0%), SiO_2 (purity 95%), MgO (purity 98%), K_2HPO_4 (purity 99%), TiO_2 (purity 99%) (Sig-ma–Aldrich), were placed in a furnace in a Pt/Rh crucible for melt-ing at temperatures between 1200 and 1450 LC, depending on composition (heating rate 8 K min^{-1}).

To produce rods, the glasses were poured into a brass mould, pre-heated at the annealing temperature [22] and then annealed. For viscosity measurements, the rods were cut by a diamond disc saw (Struers Accutom 5, cut-off wheel 330CA) and then polished (Struers Labopol-2) to obtain regular cylindrical rods with parallel faces (diameter 5 mm, length 6 mm). Other glass rods (diameter 10.5 mm, length 150 mm) were used as preforms for fibre drawing. $TiPS_{2.5}$ glass rods were also cut and polished (Struers Labopol-2) to obtain glass slices (10 _ 10 _ 1 mm) for cellular tests. All the glass samples were kept in a desiccator before use.

Glass compositions together with melting and annealing condi-tions are summarized in Table 1.

2.2. Glass viscosity

The change in glass viscosity with temperature was measured by thermomechanical analysis, using a dynamic mechanical analy-sis instrument (DMA 7 Perkin-Elmer) equipped with a thermal analysis controller (TAC7/DX) using a parallel plate measuring sys-tem. The cylindrical glass samples were heated (heating rate 5 K min^{-1}, helium atmosphere) under constant compressive force (200 mN). The sample compression

as a function of temperature was recorded until the diameter of the sample disc approached that of the plates. Finally, the viscosity was calculated through the following equation [25]:

$$\eta = 10\frac{2\pi F h^5(t)}{3V\left[\left|\frac{dh(t)}{dt}\right|\right]\left[2\pi h^3(t)+V\right]}, \quad (1)$$

where η is the viscosity in Pa s, F is the applied force in mN, h(t) is the sample thickness at time t in cm, dh(t)/dt is the compression rate at time t in cm s^{-1}, and V is the sample volume in cm^3. Then, to obtain the viscosity values in the desired temperature intervals, the Vogel–Fulcher–Tammann equation was used for viscosity data interpolation:

$$\log_{10}(\eta) = k + a/(T-b) \quad (2)$$

where η is the viscosity, T is temperature (LC), and a, b and k are constants. Constant a represents the activation energy for viscous flow or viscosity, constant b characterizes the degrees of association of molecules, and the k value represents the logarithm of a theoret-ical viscosity of completely free particles requiring no activation en-ergy for their induction into viscous flow or viscosity at an infinitely high temperature [26]. The value of k was considered to be _5, when considering the viscosity in Pa s, in accordance with the data reported in the literature [27]. To determine the values correspond-ing to a and b, the Matlab Curve Fitting Tool software was used.

2.3. Fibre drawing

The fibres were drawn following the preform drawing ap-proach, which is typically used for the production of optical glass fibres [28,29], using a drawing tower developed in-house, as de-scribed previously [22]. The preform was heated under flowing nitrogen in a furnace at the top of a drawing tower, causing the for-mation of a neck-down region, which is characterized by the stretching of the glass as a result of decreased viscosity in the heated zone. Typically, the necking down of the preform and the fibre drawing process occurs at a glass viscosity lying between 10^4 and 10^6 Pa s, corresponding to the preform drawing region [29]. Since the drawing temperature should remain below the on-set crystallization temperature of the glass in order to avoid crys-tallization on reheating, the onset temperature of the furnace (585 LC for $TiPS_0$, 620 LC for $TiPS_{2.5}$ and 690 LC for $TiPS_5$) was cho-sen as the lower temperature, which allowed the necking down of the preform and thus the fibre drawing. After necking down, the preform was fed at a constant speed into the hot zone of the furnace while a thin fibre was pulled out of the bottom of the

Table 1
Glass compositions, melting and annealing conditions.

Glass	Glass composition (mol.%)							Melting		Annealing	
	P_2O_5	CaO	Na_2O	SiO_2	MgO	K_2O	TiO_2	*T* (°C)	Time (h)	*T* (°C)	Time (h)
$TiPS_0$	50	30	9	3	3	5	–	1200	1	380	15
$TiPS_{2.5}$	50	30	9	3	3	2.5	2.5	1350	1	410	15
$TiPS_5$	50	30	9	3	3	–	5	1450	3.5	450	15

preform and collected on a cylindrical drum rotating at constant speed.

Assuming that the glass in the supercooled liquid state is an incompressible liquid, the fibre diameter was controlled during the drawing process with the following equation, obtained from the mass flow conservation law:

$$D_f = \sqrt{(D_p^2 v_p)/v_f}, \quad (3)$$

where D_f is the fibre diameter, v_f is the fibre drawing speed, D_p is the preform diameter, and v_p is the preform feeding speed. In order to obtain fibres of different diameters, different speeds, v_p and v_f, were applied. The process parameters used for fibre drawing and the cor-responding theoretical fibre diameters are reported in Table 2, to-gether with the fibre sample codes.

At the end of the drawing process, 10 fibres of each type were placed on a sample holder using adhesive tape, and the diameter was measured using a Reichert-Jung MeF3 metallurgical micro-scope equipped with Leica Qwin software for image analysis. Structural, morphological and compositional analyses on glass fi-bres were carried out by X-ray diffraction (XRD) analysis on glass powders resulting from milling the glass fibres (X'Pert Philips dif-fractometer with Bragg Brentano camera geometry and Cu K_a inci-dent radiation) and scanning electron microscopy (SEM; Quanta Inspect 200LV, Fei Company, The Netherlands). Energy dispersive spectroscopy (EDS) was also carried out on bulk glasses and as-drawn glass fibres.

2.4. Dissolution tests on glass fibres

Dissolution tests were conducted on the TiPS glass fibres of dif-ferent compositions and diameters. In order to investigate the influence of a post-drawing thermal treatment, the dissolution of both as-drawn and annealed $TiPS_{2.5}$ glass fibres with a theoretical fibre diameter of 78 lm (sample code T2-78 and T2-78-an, respec-tively) was investigated (see Table 1 for annealing conditions).

In the first set of experiments, the dissolution of the fibres was investigated in term of decrease in diameter. For each type of fibre, three samples were soaked in bi-distilled water (pH 6.0 ± 0.5) at 37 LC with a solution volume/sample area ratio of 0.1 ml mm^{-2}. The high purity of bi-distilled water allows the dissolution kinetics of the glasses to be studied, minimizing the influence of outside ions on the dissolution process. In order to obtain the desired solu-tion volume/sample area ratio, the exposed area of the fibre sample was calculated on the basis of its weight and density. For each sam-ple, fibres with diameter D_f were considered as a single cylindrical fibre with the same diameter and length L, which is the sum of the single fibre length. Thus, considering, with an approximation, that the fibres have a perfectly cylindrical shape with a completely smooth surface, the exposed surface area of the fibre sample can

Table 2
Processing parameters used for fibre drawing with the corresponding theoretical fibre diameters and fibre sample codes.

Preform feeding speed v_p (mm min^{-1})	Drawing speed v_f (m min^{-1})	Theoretical fibre diameter (μm)	Glass code	Fibre sample code
0.2	35.3	25	$TiPS_0$	T0-25
			$TiPS_{2.5}$	T2-25
			$TiPS_5$	T5-25
0.6	10.9	78	$TiPS_0$	T0-78
			$TiPS_{2.5}$	T2-78
			$TiPS_5$	T5-78
	40.8	40	$TiPS_0$	T0-40
			$TiPS_{2.5}$	T2-40
			$TiPS_5$	T5-40

be calculated as the lateral surface A_l of the cylinder with the following formula:

$$A_l = \pi D_f L = \pi D_f \left(\frac{W}{\rho}\right) \Big/ \left(\pi \frac{D_f^2}{4}\right) = (4W)/(\rho D_f), \quad (4)$$

with W the weight of the cylinder (i.e., weight of the fibre sample), and q the glass density, which is 2.573 ± 0.008 for $TiPS_0$, 2.587 ± 0.002 for $TiPS_{2.5}$ and 2.614 ± 0.007 for $TiPS_5$ [22].

At different time points (1, 3, 7, 19, 24, 30 h for $TiPS_0$, which shows faster dissolution, and 72, 144, 216, 360, 480 h for $TiPS_{2.5}$ and $TiPS_5$) the pH of the solution was measured using WTW VAR-IO Waterproof pH Meter (WTW , Weilheim, Germany) and at least three fibres were removed from the solution and dried. Refreshing of the medium was performed after pH measurement at 72, 144, 216, 360, 480 h in order to simulate the physiological fluid exchange.

For each time point, 10 measures were performed on different fibres and in different positions of the fibre length, using a Reic-hert-Jung MeF3 metallurgical microscope equipped with Leica Qwin software for image analysis, and the mean diameter of the degraded fibres D_f was calculated.

The surface modifications of the fibres due to degradation were investigated with SEM (Quanta Inspect 200LV, Fei Company, The Netherlands) and EDS analysis. T2-78 fibres were also soaked for 2 months in bi-distilled water with no refreshing of the medium and then observed by SEM.

A second set of experiments was carried out to study fibres weight loss. For each type of fibre, the samples were soaked in bi-distilled water in the same conditions used for the other disso-lution test. At different time points (3, 6 h or 6, 24 h for $TiPS_0$, which shows faster dissolution, and 72, 144 h for $TiPS_{2.5}$ and $TiPS_5$) the water was removed from three samples, the fibres were then dried overnight at 37 LC and reweighed. The weight loss percent-age of the fibres %WL was calculated with the following formula:

$$\%WL = 100(W_0 - W_f)/W_0 \qquad (5)$$

where W_0 and W_f are, respectively, the initial and final weight of the sample.

2.5. Biological tests

2.5.1. Preparation of the samples

Samples of aligned $TiPS_{2.5}$ fibres of different diameters (T2-25, T2-40 and T2-78) were prepared for biological tests. A group of fi-bres was placed on a brass plate and arranged in an aligned config-uration (Fig. 1a), and two other groups of fibres of the same type were placed transversally at the extremities, with two brass plates applying pressure over them (Fig. 1b). Thermal treatment (510 LC, 1 h, heating rate 12 K min^{-1}) was performed in a furnace (Carbolite 1200) in order to allow the joining of the different group of fibres to obtain a sample with a stable aligned configuration of fibres (_1.2 _ 1.5 mm, 15–20 mg), as shown in Fig. 1c.

2.5.2. NOBEC line

In the first set of experiments, a 3-day incubation of the NOBEC line, derived from primary cells dissociated from neonatal rat olfactory bulb and immortalized by retroviral transduction of SV40 large T antigen [30], was carried out in the presence of sam-ples of $TiPS_{2.5}$ aligned fibres of different diameters (T2-25, T2-40 and T2-78). Glass coverslips and $TiPS_{2.5}$ slices were used as controls during the cellular test. The test was performed in triplicate.

About 20,000 cells were cultured in six-well culture plates. NO-BEC were grown in monolayer at 37 LC in a humidified atmosphere of 5% CO_2/air, in Dulbecco's modified Eagle's medium supple-mented with 100 units ml^{-1} penicillin, 0.1 mg ml^{-1} streptomycin,

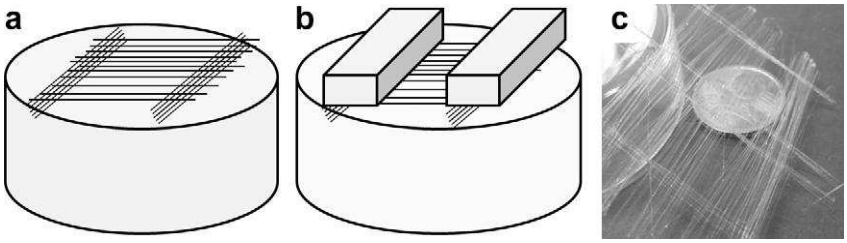

Fig. 1. Preparation of $TiPS_{2.5}$ fibres samples for biological tests. Before thermal treatment (a) a group fibres was arranged in aligned configuration on a brass plate and two other groups of fibres were placed transversally, (b) two brass plate were placed on the transversal fibres, imparting a pressure over them; (c) samples obtained.

1 mM sodium pyruvate, 2 mM L-glutamine and 10% heat-inacti-vated fetal bovine serum (FBS; Invitrogen) in the presence of the samples. After 3 days of incubation, the samples were observed di-rectly in the well, using an inverted biological microscope and also a confocal microscope after immunofluorescence reaction. For immunofluorescence, some samples were incubated with primary antibody against S100 (polyclonal, rabbit, 1:600, Sigma, St Louis, MO), a glial protein expressed by NOBEC cells. After washing in PBS, samples were then incubated with CY3 secondary antibody (a-rabbit IgG, Jackson immunoresearch Europe, Suffolk, UK). Confo-cal imaging was carried out with a LSM 510 confocal laser micros-copy system (Zeiss, Jena, Germany), which incorporates two lasers (argon and HeNe) and is equipped with an inverted Axiovert 100 M microscope. SEM analysis (Quanta Inspect 200LV, Fei Company, The Netherlands) was also performed after fixation with glutaral-dehyde (2.5%), washing in PBS and dehydration in ethanol (from 50% to 100%).

2.5.3. DRG neurons

In a second set of experiments a 3-day incubation of DRG disso-ciated neurons from adult rats was carried out in the presence of $TiPS_{2.5}$ aligned fibres of different diameters (T2-25, T2-40, T2-78). Glass coverslips and $TiPS_{2.5}$ slices were used as controls during the cellular test. The test was carried out in triplicate.

Adult female Wistar rats (Charles River Laboratories, Milan, Italy) weighing _190–220 g were used for this study. Rats were sacrificed by a lethal i.m. injection of tiletamine + zoletil. The ver-tebral column was surgically dissected, and the vertebral bodies were cut off and removed in order to reach the spinal cord. Briefly, using fine scissors, the vertebral canal was accessed, performing a double cut on both sides of the vertebral bodies. The ventral access through the vertebral bodies does not interfere with the DRG lo-cated along the dorsal roots. All procedures were performed in accordance with the Ethic Committee and European Communities Council Directive of 24 November 1986 (86/609/EEC). Adequate measures were taken to minimize pain and discomfort, taking into account human endpoints for animal suffering and distress.

DRG were dissociated using enzyme digestion [31]. Briefly, DRG were removed and enzymatically dissociated in Ham's F12 med-ium (Invitrogen, Milan, Italy) containing 0.125% collagenase Type IV (Sigma, St. Louis, MO) and incubated for 1 h (37 LC, 5% CO_2) for two cycles and treated with 0.25% trypsin (Sigma, St. Louis, MO) for 30 min (37 LC, 5% CO_2). The trypsin was inactivated with 33% FBS, and the ganglia were mechanically dissociated by gentle trituration using a glass pipette, passed through a 70 lm pore size filter (BD Biosciences, Milan, Italy) and centrifuged (200g, 5 min). The trituration and centrifugation was repeated to ensure the DRG had been dissociated. Cells were re-suspended in Ham's F12 medium and centrifuged (600g, 10 min) with 15% bovine serum albumin. Dissociated neurons were re-suspended in Ham's F12 medium, seeded 50% confluent on pre-coated glass coverslips, glass slice of $TiPS_{2.5}$ and glass fibre samples with 2 lg ml^{-1} lami-

nin-1 (Sigma) [31], and maintained in defined serum-free medium (SFM) [32] at 37 LC with 5% CO_2.

After 3 days of incubation, the samples were observed directly in the well using an inverted biological microscope and also a con-focal microscope after immunofluorescence reaction. For immuno-fluorescence, the samples were rinsed in PBS, blocked with normal serum (1%) (the use of a normal serum made in the same species of the secondary antibody is recommended) for 1 h and then incu-bated overnight with the primary antibody. The samples were incubated with primary antibody against beta-tubulin (monoclo-nal, mouse, 1:1000, Sigma, St. Louis, MO, USA), which specifically recognizes neurons. After primary antibody incubation, samples were washed three times in PBS and incubated for 1 h in a solution containing the secondary antibody (ALEXA 488 a-mouse) conju-gated with a fluorophore and selected in order to recognize the species of primary antibodies. After three washes in PBS, samples were finally mounted with a Dako fluorescent mounting medium and stored at 4 LC before being analysed on a LSM 510 confocal la-ser microscopy system (Zeiss, Jena, Germany). SEM analysis (Quan-ta Inspect 200LV, Fei Company, The Netherlands) was also performed after fixation with glutaraldehyde (2.5%), washing in PBS and dehydration in ethanol (from 50% to 100%).

3. Results and discussion

3.1. Glass viscosity

The results of the glass viscosity measurement are reported in Fig. 2. It is possible to observe the viscosity of the different TiPS glasses (continuous line), calculated from the sample compression as a function of the temperature using Eq. (1), and the correspond-ing regression curves (dotted line), calculated using Eq. (2). Consid-ering the same temperature values, the viscosity increases with

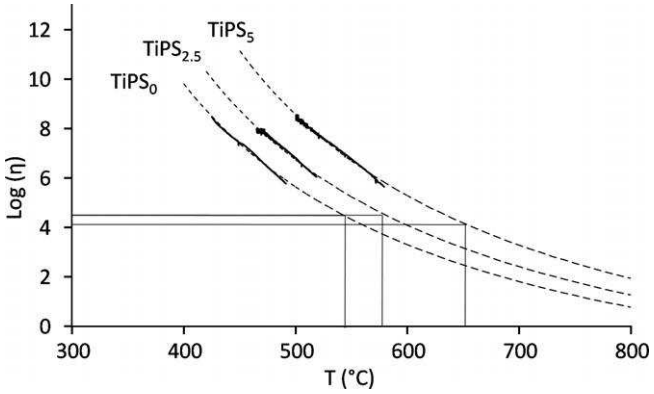

Fig. 2. Viscosity of the different TiPS glasses (continuous line), calculated from the sample compression as a function of the temperature and the corresponding regression curves (dotted line). The drawing temperature for the different glasses and the corresponding viscosity are also graphically indicated.

increase in the TiO_2 content in the glass. This can be attributed to the influence of TiO_2 on the glass structure, with the formation of ionic cross-links between phosphate chains or Ti–O–P covalent bonds; in fact, both of them are supposed to reinforce the glass structure [33,34]. This is also in accordance with the results of pre-vious studies on TiPS glasses, in which TiO_2 was found to stabilize the glass network, causing an increase in glass characteristic tem-peratures and density and a decrease in glass solubility [22,23].

3.2. Glass fibres

Several tens of metres of fibres were successfully drawn from all TiPS glasses following the preform drawing approach. The main constraint when drawing fibre using the preform drawing ap-proach is that it involves reheating of the glass preform above the glass transition temperature. Therefore, the drawing tempera-ture should remain below the onset crystallization temperature (T_c), to avoid crystallization on reheating. To avoid disturbance of the drawing process, the system did not have any instrumentation to measure the glass preform temperature directly. However, based on the authors' experience using other glass systems, a glass preform temperature _40 K lower than the onset furnace temper-ature should be expected. Basically, considering the drawing tem-peratures reported in Section 2.3, the temperature of the preform was _545 LC for $TiPS_0$, 580 LC for $TiPS_{2.5}$ and 650 LC for $TiPS_5$, which are below the respective T_c of the glasses (552 LC, 640 LC and 687 LC [22]). As it is possible to observe in Fig. 2, the chosen draw-ing temperatures correspond to a viscosity of $\_10^4$ Pa s and, more specifically, $\log_{10}(g)$ resulted to be 4.5 for $TiPS_0$ and $TiPS_{2.5}$ and 4.2 for $TiPS_5$.

SEM analyses showed that the fibres had well-defined and reg-ular shapes and presented surfaces free from defects or crystalline phases, as confirmed also by the XRD analysis results (data not shown). The fibres were free of contamination, as no difference was found between the EDS spectra of the bulk glass (Fig. 3) and those of all the glass fibres types (data not shown).

The diameters of the fibres obtained are reported in Table 3 in comparison with the theoretical values obtained through Eq. (3). The diameters obtained compare favourably with the theoretical ones, with a maximum difference of _4 lm between the mean measured values and the theoretical ones, obtained for sample T0-78, and only 1 lm for most of the fibres. Moreover, the standard deviation of the measured diameters showed a maximum value of 3 lm, obtained for sample T2-25, and only 1–2 lm for the other ones. These data confirm that the fibre diameter can be easily set on the basis of the processing parameters, and that it will remain quite constant during the whole drawing process, demonstrating the reproducibility of the process along the drawing time.

Table 3
Theoretical and measured fibre diameters (mean ± SD) obtained for the different fibre samples.

Theoretical fibre diameter (μm)	Fibre sample code	Measured diameter (μm)
25	T0-25	28 ± 1
	T2-25	25 ± 3
	T5-25	27 ± 1
40	T0-40	41 ± 1
	T2-40	41 ± 2
	T5-40	41 ± 1
78	T0-78	82 ± 1
	T2-78	78 ± 2
	T5-78	79 ± 1

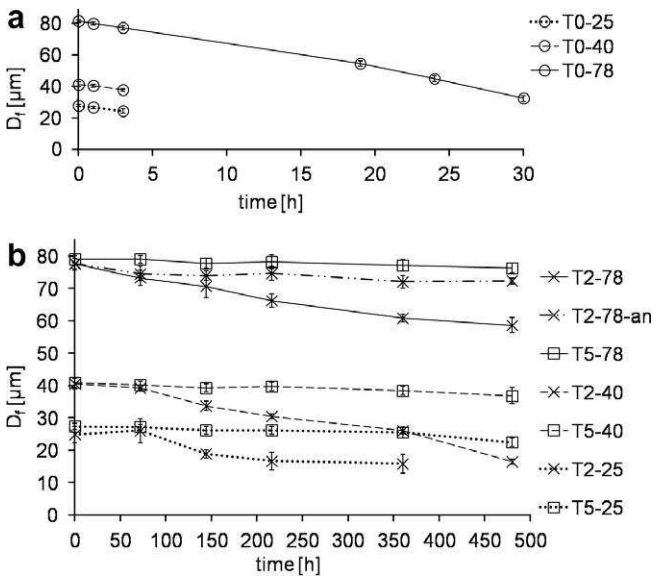

Fig. 4. Fibre diameter (D_f) change in (a) $TiPS_0$ samples and (b) $TiPS_{2.5}$ and $TiPS_5$ samples.

3.3. Dissolution tests on glass fibres

The fibre diameter of the glass fibres during the dissolution test (D_f) is shown in Fig. 4a and b, and the weight loss percentage (%WL) is reported in Fig. 5a–c. All $TiPS_5$ fibre samples (T5-25, T5-40 and T5-78) and $TiPS_{2.5}$ fibre samples with the highest diameters (T2-40 and T2-78) were still present in solution until the end of the first dissolution test (480 h), while the T2-25 samples had almost disappeared at the end of the dissolution test; after 480 h, only a

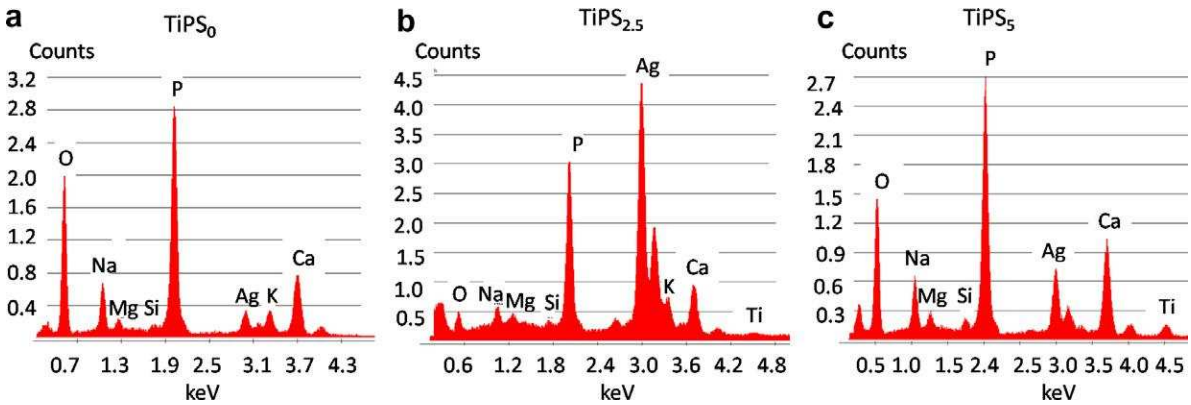

Fig. 3. EDS spectra of (a) $TiPS_0$, (b) $TiPS_{2.5}$ and (c) $TiPS_5$ bulk glass.

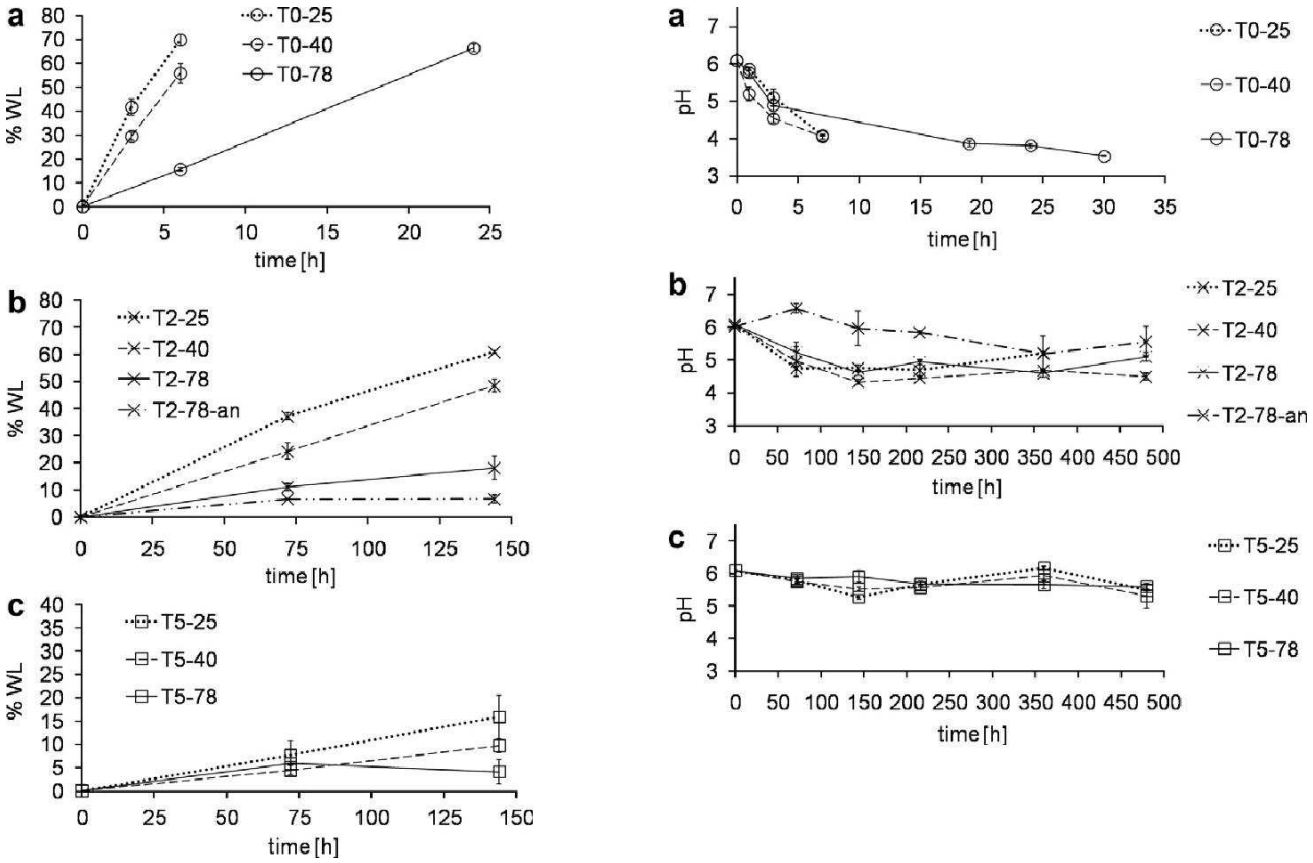

Fig. 5. Weight loss percentage (%WL) of (a) $TiPS_0$ (b) $TiPS_{2.5}$ and (b) $TiPS_5$ fibres during dissolution in bi-distilled water.
Fig. 6. Change in pH of the medium during dissolution of (a) $TiPS_0$ (b) $TiPS_{2.5}$ and (b) $TiPS_5$ fibres in bi-distilled water. Refreshing of the medium was performed after pH measurement at 72, 144, 216, 360 and 480 h.

few fibres were still present in solution, and measurement of the fibre diameter was not possible. $TiPS_0$ fibre samples disappeared in shorter times, after 7 h for T0-25 and T0-40, and after 30 h for T0-78. The slight increase in D_f measured for T2-25 sample at 72 h was not a statistically significant difference ($p > 0.05$). As re-gard the influence of the composition on the glass dissolution, it is possible to observe a decrease in glass solubility with increase in TiO_2 content, as shown by the slower change in D_f and %WL, passing from $TiPS_0$ to $TiPS_{2.5}$ and finally to $TiPS_5$. These results can be attributed to the stabilizing effect of TiO_2 on the glass net-work due to the formation of ionic cross-links between phosphate chains or Ti–O–P covalent bonds [33,34], as discussed in Sec-tion 3.1, in accordance with previous studies by the authors and with other studies reported in the literature [22,23,34–37].

As regards the influence of fibre diameter, the results of the dis-solution tests should be discussed considering that phosphate glass dissolution, being a surface erosion process, is strongly dependent on the glass exposed surface. Fibres of the same glass type (what-ever the initial diameter) showed a similar diameter change profile during dissolution (Fig. 4). This can be explained by considering that the diameter change profile is directly related to the weight loss per unit area of the fibre (i.e., the weight per unit area of the fibre can be expressed as $W/A_l = (D_f p)/4$, derived from Eq. (4)), which depends mainly on the glass composition. In contrast, %WL showed higher values for the fibres with smaller diameters (Fig. 5). Since the specific surface area ($A_l/W = 4/(qD_f)$) is inversely propor-tional to D_f, fibres with smaller diameters showed higher %WL. The slight decrease in %WL measured for sample T5-78 at 144 h was not a statistically significant difference ($p > 0.05$).

In this study, the influence of an annealing treatment on the glass fibre dissolution was investigated. The annealed fibres (T2- 78-an) showed slower dissolution in terms of diameter decrease and weight loss percentage compared with their as-drawn coun-terpart fibres (T2-78), as observed in Figs. 4 and 5.

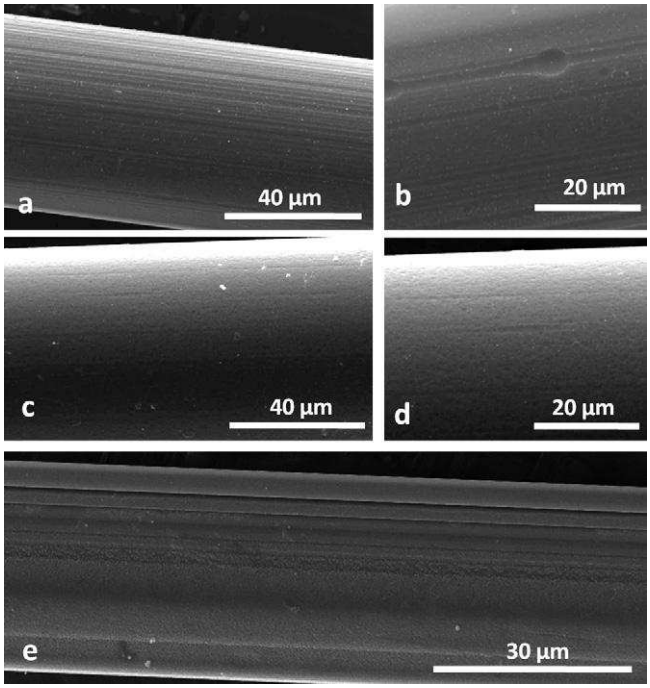

Fig. 7. SEM images showing the surface modifications of the fibres due to dissolution in bi-distilled water: (a) and (b) as-drawn $TiPS_{2.5}$ fibres (T2-78) after 480 h (20 days); (c) and (d) annealed $TiPS_{2.5}$ fibres (T2-78-an) after 480 h (20 days); (e) as-drawn $TiPS_{2.5}$ fibres (T2-78) after 2 months.

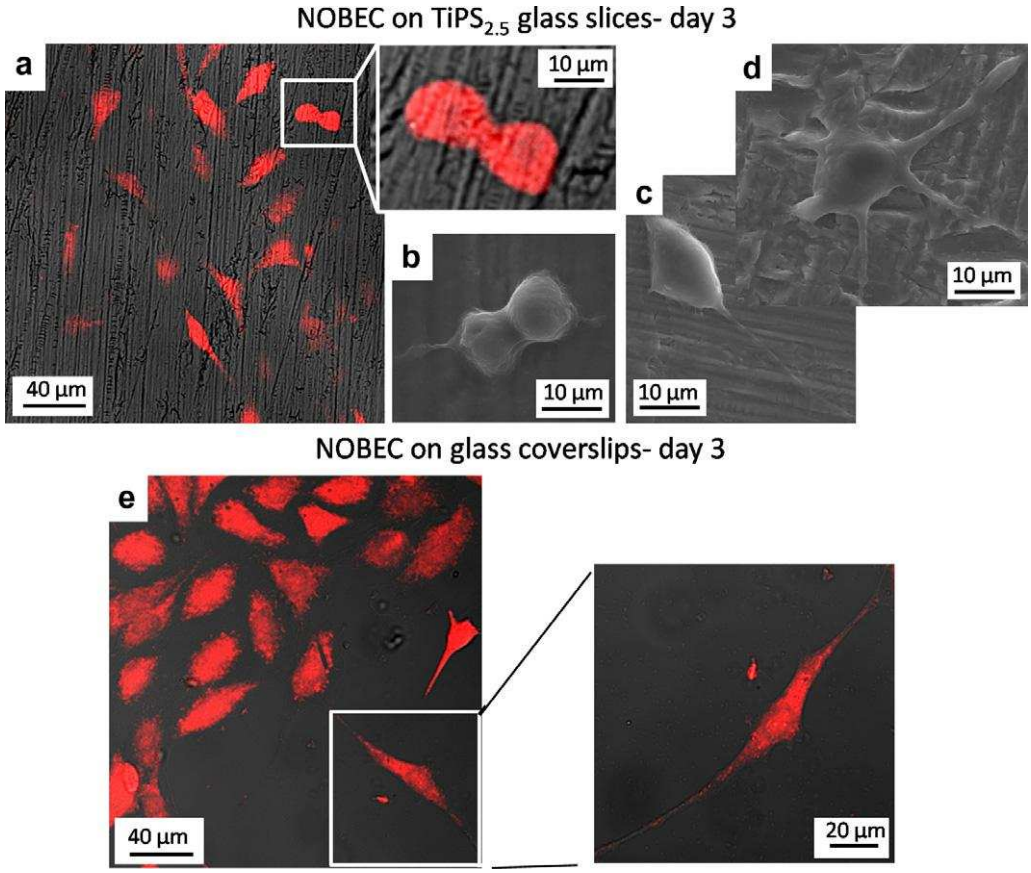

Fig. 8. NOBEC cells after 72 h (3 days) incubation in the presence of the control $TiPS_{2.5}$ slices (a)–(d) and glass coverslips (e). (a) Cells with spread morphology and after mitosis (image at higher magnification) on $TiPS_{2.5}$ glass slices, observed on a confocal microscope; (b) cells after mitosis on $TiPS_{2.5}$ glass slices, observed by SEM; (c) and (d) cells showing some processes extending from the cells to the surface of $TiPS_{2.5}$ glass slices, observed by SEM; (e) cells with spread morphology observed on control glass coverslips, observed on a confocal microscope. For immunofluorescence reaction, primary antibody S100 and CY3 secondary antibody were used.

Other authors in the literature investigated the influence of a heat treatment on the dissolution of phosphate glass fibres, and found similar results [38–40]. Choueka et al. [38] studied the influence of heat treatments on the dissolution of phosphate glass fibres containing zinc and iron. The authors observed that the degradation rates for the fibres were inversely proportional to the annealing temperature. Cozien-Cazuc et al. [39] found that the annealing treatment re-duced the dissolution of glass fibres with composition $40P_2O_5$– $20Na_2O$–16CaO–24MgO (mol.%) in distilled water, with a differ-ence of an order of magnitude in the dissolution rate calculated on the first 24 h. The lower dissolution rate of the annealed fibres could be due to stabilization of the glass structure by the relieving of the residual stresses arising from drawing. Cozien-Cazuc et al. [40] proposed that the annealed fibres, losing part of the oriented structure imparted by the fibre drawing via relaxation of the poly-meric chains, have a more durable structure, less susceptible to stress corrosion effects.

A decrease in the pH value in the soaking medium was observed during dissolution, probably due to the presence of acidic dissolu-tion products deriving from the breakdown of the polyphosphate chains of the glass in solution (Fig. 6). In fact, the change in pH was more evident with increasing glass solubility. The introduction of TiO_2 in the glass composition and the consequent stabilization of the glass network could prevent excessive lowering of pH during dissolution [22,23]. Also the annealing treatment, stabilizing the glass structure and decreasing the glass dissolution, can limit the change in pH during fibre dissolution, as it is possible to see by comparing the results of the annealed fibres (T2-78-an) and their corresponding as-drawn fibres (T2-78) in Fig. 6. However, it should be considered that the present results refer to glass dissolution in bi-distilled water, which is a non-buffered solution and so is not able to counterbalance the change in pH. In a previous study, the dissolution of TiPS bulk glass in bi-distilled water caused a de-crease in pH similar to that observed for TiPS fibres in this study; however, TiPS bulk glass soaked in buffered solutions, such as Tris–HCl and citric acid, in the same experimental conditions maintained constant pH during dissolution, even when a weight loss similar to those obtained in bi-distilled water was reached [22]. For this reason, analogous results can be expected in physio-logical fluids, which are buffered, where negligible pH lowering can be expected.

SEM analysis of the glass fibres showed that many straight fur-rows and hollows, aligned with the fibre axis direction and increas-ing in dimension with time, appeared on the surface of the degraded fibres. As an example, Fig. 7a and b shows the morphol-ogy of T2-78, while Fig. 7c and d shows the morphology of T2-78-an fibres at the end of the dissolution test. This morphology reflects the oriented glass structure arising from the drawing process, in which phosphate chains are aligned along the fibre axis. Also Coz-ien-Cazuc et al. [39] found aligned holes on degraded phosphate glass fibres, and they observed that this may be related to the drawing process. Stockhorst and Brückner [41] hypothesized that the drawing stress acting on the fibres during fibre drawing gives rise to a structural anisotropy, with phosphate glass fibre showing orientation of chains in the axial fibre direction. The authors sup-posed that the non-bridging oxygens are oriented mainly in the ra dial direction, while the bridging oxygens are connecting the PO^3_4– chain structure units in the fibre axis direction.

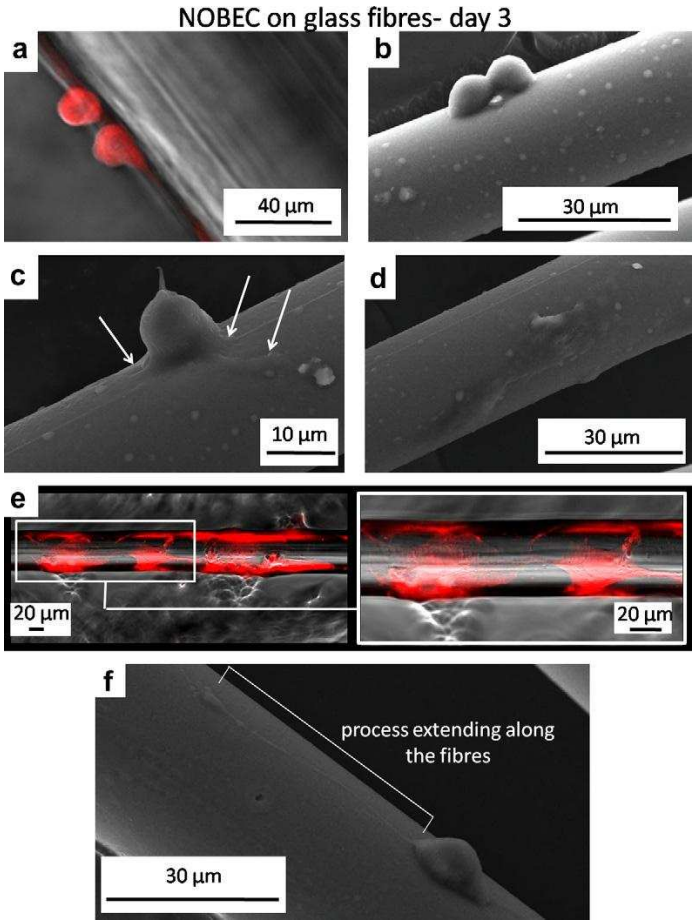

Fig. 9. NOBEC cells after 3 days incubation in the presence of $TiPS_{2.5}$ glass fibres. NOBEC cells showing active proliferation (a) on T2-78 glass fibre (confocal microscope image) and (b) on T2-25 glass fibre (SEM image); (c) NOBEC cell adhering to the surface of a fibre (T2-25) with the cytoplasmatic processes extending from the cells to the fibre surfaces (indicated by arrows); (d) adhered NOBEC cell spread on the surface a fibre (T2-25); (e) confocal microscope images at different magnifications showing NOBEC cells spread on the glass surface, enveloping glass fibre (T2-25) (for immunofluorescence reaction, primary antibody S100 and CY3 secondary antibody were used). (f) SEM image showing NOBEC cell adhered on the fibre surfaces with a process extending along a glass fibre (T2-40).

The furrows were less numerous in annealed fibres than in as-drawn ones. This could be due to the slower dissolution of the an-nealed fibres, but also to the above discussed structure relaxation following the annealing treatment which led to a less oriented chain structure of the glass. In fact, thermal agitation during heat treatment will relax the polymer chains, promoting a more stable configuration [7,39,40].

Numerous studies in the literature describe a loss of structural integrity of the phosphate glass fibres during dissolution [7,38– 40,42,43]. Cozien-Cazuc et al. [39,40] observed the formation of an outer hydrated layer and delamination during dissolution on both as-drawn and annealed glass fibres with composition $40P_2O_5$–$20Na_2O$–16CaO–24MgO (mol.%). Choueka et al. [38] ob-served thin shells peeling off the outer coating of phosphate glass fibres containing zinc and iron after 2 months in physiological solutions. Abou Neel et al. [42] observed the formation of micro-tubes through the degradation of glass fibre with composition $50P_2O_5$–0.30 CaO–(0.17–0.15)Na_2O–(0.03–0.05)Fe_2O_3 (mol.%) after 3 months in deionized water. Rinehart et al. [43] observed a fragmented surface on phosphate glass fibres containing iron during dissolution in phosphate buffered saline solution. TiPS fibres, de-spite the above discussed change in surface morphology, main-tained their structural integrity during the whole dissolution period, without breaking. Even after 2 months in bi-distilled water without any refresh, T2-78 fibres maintained their shape, showing only a diameter decrease (final diameter _31 lm) and the pres-ence of aligned furrows on the surface (Fig. 7e). Moreover, the dis-solution of all TiPS fibre samples was congruent, since no compositional change took place during dissolution of the fibres and in fact no difference was found between the EDS spectra of the degraded fibres and those of the bulk glasses (Fig. 3).

3.4. Biological tests

3.4.1. NOBEC line

NOBEC cells were found to be well spread on the surface of $TiPS_{2.5}$ glass slices (Fig. 8a, c and d), with a cell morphology compa-rable with those obtained on the control glass coverslips (Fig. 8e). Cells after mitosis were observed on $TiPS_{2.5}$ glass slices, as shown in Fig. 8a (higher magnification) and Fig. 8b

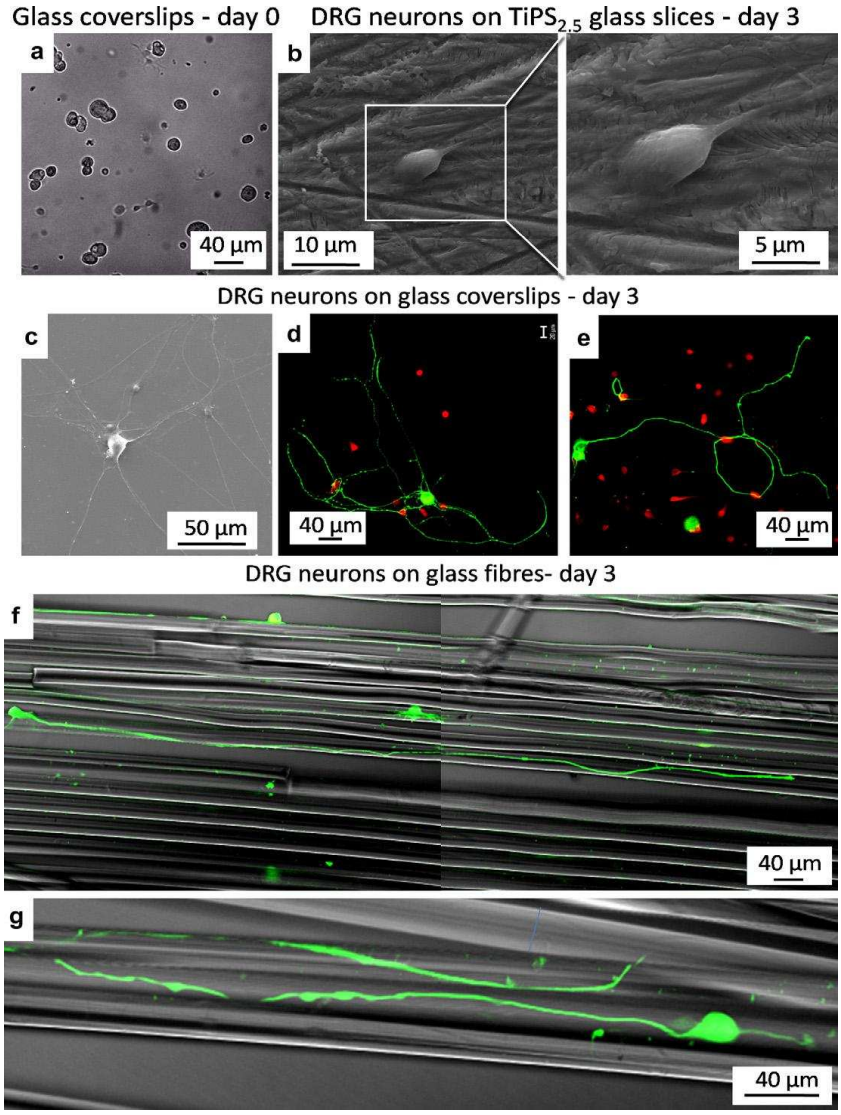

Fig. 10. (a) Image of inverted biological microscope showing DRG neuron on a glass coverslips at day 0, presenting rounded morphology; (b) SEM image of DRG neuron after 3 days incubation on $TiPS_{2.5}$ glass slices; (c) SEM image and (d) confocal microscope images showing DRG neurons after 3 days incubation on glass coverslips. Dendrites extend from the cell body in all direction (multipolar morphology); (e) confocal microscope images showing DRG neurons after 3 days incubation on glass coverslips, showing long neurites; (f) and (g) DRG neurons on glass fibres (T2-25), presenting long neurites extended along the fibre axis direction. For immunofluorescence reaction, primary antibody beta-tubulin and ALEXA 488 a-mouse secondary antibody were used.

Different maturation processes were also observed for NOBEC cells incubated in the presence of glass fibres. NOBEC cells showed active proliferation on glass fibres, as shown in Fig. 9a and b. More-over, the cells adhered to the material, presenting cytoplasmatic processes extending toward the fibre surface (Fig. 9c). Most of the S100-positive cells in contact with the fibres presented elon-gated shape and were well spread on the surface, enveloping the glass fibres (Fig. 9d and e). Some of adhering cells presented cyto-plasmic processes extending along the fibres (Fig. 9f). Cell adhesion is important, since it is one of the necessary conditions for cell migration. All attachment-dependent cell types, from osteoblasts to neurons, migrate across surfaces by adhering, contracting fol-lowed by moving as a result of contractile forces [44]. The migra-tion of glial cells is fundamental in the nerve regeneration process [45]. For large nerve defects, exogenous supports are needed to enable the regenerating fibres to cross the nerve gap, [18]. Microstructured biomaterial filaments were shown to provide a better topography, promoting Schwann cells and axon alignment, which in the perspective of in vivo employment may improve nerve regeneration across the tube [46,47].

No clear influence of different $TiPS_{2.5}$ fibre diameters on NOBEC cell interaction with the fibres was observed.

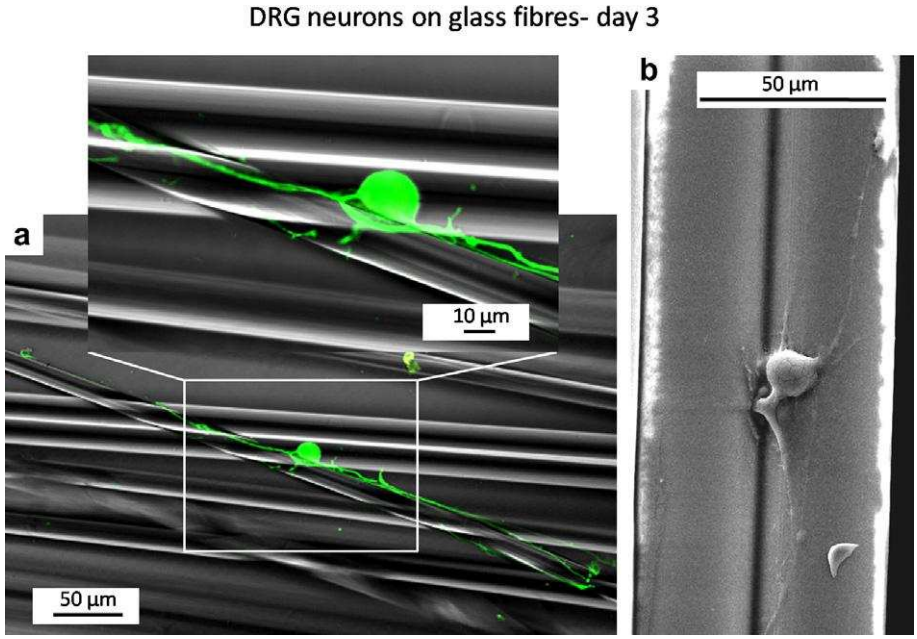

Fig. 11. DRG neuron showing a pseudounipolar morphology (a) on a glass fibre (T2-25) analysed using a confocal microscope at different magnifications and (b) on a T2-40 fibre (SEM image) after 3 days in culture.

3.4.2. DRG neurons

Usually, when DRG dissociated neurons are seeded in culture, they are round in shape, with no neurites leaving the cell body: e.g., the DRG neurons on control glass coverslips at day 0 as seen in Fig. 10a. Between 1 and 3 days in culture, postmitotic neurons initially extend and retract in all directions multiple short neuritic processes, which are comparable in length and growth rate [48], as shown in Fig. 10c and d. Finally, in neurons that elaborate an axon, one neurite outgrows the others. This first long B-tubulin-positive neurite continues to growth without tapering and becomes the sin-gle axon, as shown in Fig. 10e. The neuronal shape changed from multipolar to bipolar as a consequence of the normal neuronal maturation.

It was not possible to clearly observe DRG neurons after 3 days of incubation on the control $TiPS_{2.5}$ glass slices. SEM analysis of the samples clearly identified the cell body, whereas it was not possi-ble to distinguish the neurites from the glass surface, owing to the numerous furrows arising from the glass polishing process. How-ever, the neuronal processes appeared to be well integrated with the dissolving glass surface, as shown in Fig. 10b.

All the neurons showed a bipolar shape and presented one or two long growing B-tubulin-positive axons, as shown in Fig. 10f and g. In general, the long neurites observed for the neurons on the glass fibres are longer than those observed on glass coverslips (see Fig. 10e for comparison). Thus, the presence of the fibres seemed to be the cause of the polarization of neurons, meaning that one neurite, generally the longest, became the axon. In vivo, cues in the local environment are likely to specify a particular direction for neurite outgrowth, while, under culture conditions which lack directional information, the choice of neurite that be-comes the axon appears to be stochastic [48]. Interestingly, in this study, DRG neurons cultured on $TiPS_{2.5}$ glass fibre samples showed long neurites extending along the fibre axis direction (Fig. 10f and g). This indicates that the fibres are likely not only to promote the polarization of neurons, but also to impart directionality to the axon growth. Directed cell growth and migration are fundamental to many physiological processes such as tissue morphogenesis and wound healing and is also frequently desired in a multitude of tis-sue engineering applications. In particular, directed growth of neu-rites for regeneration of peripheral and central nervous system tissue is desirable [44].

Smeal et al. [49] studied the directional growth of DRG neurons on polymeric fibres with diameters ranging between 35 and 500 lm. They found that substrate curvature is sufficient to influ-ence the directional outgrowth of DRG neurites. The authors pro-posed that cell processes sustain a bending-induced strain when extending on a cylindrical substrate, which is withstood by their cytoskeleton, the primary mechanical structure of the cell. They demonstrated that the mean direction of neurite outgrowth is aligned with the direction of minimum principle curvature. This could be a possible explanation for the different neuronal morphol-ogy on the flat glass coverslips and $TiPS_{2.5}$ glass fibres.

The authors also hypothesized that cell bending stiffness may limit outgrowth patterns as a function of decreasing diameter. In fact, they found that the tendency of neurite outgrowth along the axis direction of polymeric fibres increased with decreasing fibre diameter. In this study, as for NOBEC cells, no clear influence of dif-ferent $TiPS_{2.5}$ fibre diameters was observed on the basis of the re-sults of the interaction of DRG neurons with the fibres.

Some of the neurons on the glass fibres samples showed a pseu-do-unipolar morphology, as detectable in Fig. 11a and b. In fact, for dorsal root ganglion, the evolution of the neuronal shape after ax-onal outgrowth leads to the formation of a single dendrite process, which partially fuses with the axon to produce the double branched processes typical of the pseudo-unipolar neurons [48].

4. Conclusions

All TiPS glasses were successfully drawn into fibres with micro-metric diameters, using the preform drawing approach. The draw-ing process allowed easy and precise tailoring of the fibre diameter, acting on the process parameters, obtaining fibres with well-de-fined and regular shapes and surfaces free from defects or crystal-line phases.

The solubility showed a decrease with increasing TiO_2 content in the glass composition, owing to its stabilizing effect. The results also showed that heat treatment of the fibres, such as annealing treatment, is able to stabilize the glass structure, resulting in a de-crease in fibre solubility. Fibres of the same glass type showed increasing weight loss percentage with decreasing diameters, ow-ing to the different specific surface area, but a similar diameter change profile. Thus the fibre diameter, together with glass compo-sition and heat treatment, are the determining factors for the final resorption time of the samples. The possibility of tailoring the dis-solution rate of glass samples acting on these factors is very impor-tant when designing a biomedical construct with a desired resorption time.

Moreover, these data demonstrated that the glass fibres main-tain their structural integrity and composition during dissolution. This is important in view of their potential use for biomedical applications. In fact, the fibres are expected only to decrease in size during degradation, without any other unexpected

changes in their shape and properties.

The aim of the biological tests was to assess fibres biocompati-bility and to investigate the interaction of the cells with the fibres in view of their potential use in the synthesis of a device for the treatment of peripheral nerve damage. The results obtained con-firm the hypothesis of biocompatibility of $TiPS_{2.5}$ glass fibres and support the view that they are permissive substrates for glial cell adhesion and alignment as well for axonal growth. In fact, glial cells were found to adhere well to the surface of $TiPS_{2.5}$ glass slices as well as DRG neurons. Interestingly, all neurons adherent to the glass fibres grew and extended long axons along the fibre axis direction. Thus, the authors believe that the aligned configuration of the fibres forms an anisotropic environment, which provides a directional cue for axonal growth. Moreover, the straight furrows aligned in the fibre axis direction, formed as a consequence of the fibres dissolution, may also play a role in the topographic direc-tion of growing axons during peripheral nerve regeneration.

Numerous studies have demonstrated that the presence of a scaffold with an anisotropic structure enables faster or better nerve regeneration [15,18,50]. Bunting et al. [15] found that silastic con-duits filled with aligned silica-based (Bioglass 45S5) glass fibres enhanced axonal regrowth across a 0.5 cm interstump gap in the sciatic nerves of adult rats 4 weeks after nerve lesion. The results were comparable with those obtained with autograft.

Supported by these promising findings, the potential combina-tion of $TiPS_{2.5}$ glass fibres with a polymeric nerve guidance tube, aligning the fibres in the tube axis direction, will be the subject of further studies focusing on clinical treatment of peripheral nerve damage.

Acknowledgements

The authors thank Dr Jacobberger (Comprehensive Cancer Cen-ter, Case Western Reserve University, 10900 Euclid Avenue, Cleve-land, OH 4106-4944, USA) who kindly provided the NOBEC cell line. This work was supported by Grants from the Regione Pie-monte (‘‘Bando Ricerca Sanitaria Finalizzata 2008’’). Dr Stefania Raimondo is the recipient of a PostDoc Grant partially funded by the Regione Piemonte (‘‘Azione Contenimento del Brain Drain’’).

References

1) Bunker BC, Arnold GW, Wilder JA. Phosphate glass dissolution in aqueous solutions. J Non-Cryst Solids 1984;64(3):291–316.

2) Gao H, Tan T, Wang D. Effect of composition on the release kinetics of phosphate controlled release glasses in aqueous medium. J Control Release 2004;96:21–8.

3) Knowles JC. Phosphate based glasses for biomedical applications. J Mater Chem 2003;13:2395–401.

4) Abou Neel EA, Mizoguchi T, Ito M, Bitar M, Salih V, Knowles JC. In vitro bioactivity and gene expression by cells cultured on titanium dioxide doped phosphate-based glasses. Biomaterials 2007;28:2967–77.

5) Sanzana ES, Navarro M, Macule F, Suso S, Planell JA, Ginebra MP. Of the in vivo behavior of calcium phosphate cements and glasses as bone substitutes. Acta Biomater 2008;4:1924–33.

6) Abou Neel EA, Knowles JC. Physical and biocompatibility studies of novel titanium dioxide doped phosphate-based glasses for bone tissue engineering applications. J Mater Sci Mater Med 2008;19:377–86.

7) Ahmed I, Parsons AJ, Palmer G, Knowles JC, Walker GS, Rudd CD. Weight loss, ion release and initial mechanical properties of a binary calcium phosphate glass fibre/PCL composite. Acta Bimater 2008;4:1307–14.

8) Vitale-Brovarone C, Baino F, Bretcanu O, Vernè E. Foam-like scaffolds for bone tissue engineering based on a novel couple of silicate–phosphate specular glasses: synthesis and properties. J Mater Sci Mater Med 2009;20:2197–205.

9) Leonardi E, Ciapetti G, Baldini N, Novajra G, Vernè E, Baino F, et al. Response of human bone marrow stromal cells to a novel phosphate glass-ceramic for tissue engineering applications. Acta Biomater 2010;6:598–606.

10) Bitar M, Salih V, Mudera V, Knowles JC, Lewis MP. Soluble phosphate glasses: in vitro studies using human cells of hard and soft tissue origin. Biomaterials 2004;25:2283–92.

11) Bitar M, Knowles JC, Salih V, Lewis MP. Biocompatible phosphate glass fibre scaffolds Engineering of the hard/soft tissue interface. Eur Cell Mater 2004;7(1):26.

12) Bitar M, Knowles JC, Lewis MP, Salih V. Soluble phosphate glass fibres for repair of bone–ligament interface. J Mater Sci Mater Med 2005;16:1131–6.

13) Ahmed I, Collins CA, Lewis MP, Olsen I, Knowles JC. Processing, characterisation and biocompatibility of iron-phosphate glass fibres for tissue engineering. Biomaterials 2004;25:3223–32.

14) Shah R, Sinanan ACM, Knowles JC, Hunt NP, Lewis MP. Craniofacial muscle engineering using a 3-dimensional phosphate glass fibre construct. Biomaterials 2005;26:1497–505.

15) Bunting S, Di Silvio L, Deb S, Hall S. Bioresorbable glass fibres facilitate peripheral nerve regeneration. J Hand Surg Brit Eur 2005;30B(3):242–7.

16) Navarro X, Vivó M, Valero-Cabré A. Neural plasticity after peripheral nerve injury and regeneration. Prog Neurobiol 2007;82:163–201.

17) Belkas JS, Shoichet MS, Midha R. Axonal guidance channels in peripheral nerve regeneration. Oper Tech Orthop 2004;14(3):190–8.

18) Bellamkonda RV. Peripheral nerve regeneration: an opinion on channels, scaffolds and anisotropy. Biomaterials 2006;27:3515–8.

19) Battiston B, Raimondo S, Tos P, Gaidano V, Audisio C, Scevola A, et al. Chapter tissue engineering of peripheral nerves. Int Rev Neurobiol 2009;87:227–49.

20) Meek MF, Coert JH. US food and drug administration/conformit Europe-approved absorbable nerve conduits for clinical repair of peripheral and cranial nerves. Ann Plast Surg 2008;60(4):466–72.

21) Pabari A, Yang SY M, Seifalian A, Mosahebi A. Modern surgical management of peripheral nerve gap. J Plast Reconstr Aes 2010;63:1941–8.

22) Vitale-Brovarone C, Novajra G, Milanese D, Lousteau J, Knowles JC. Novel phosphate glasses with different amount of TiO_2 for biomedical applications. Dissolution tests and proof of concept of fibre drawing. Mat Sci Eng C 2011;31(2):434–42.

23) Novajra G, Vitale-Brovarone C, Knowles JC, Maina G, Aina V, Ghigo D, et al. Effects of TiO_2-containing phosphate glasses on solubility and in vitro biocompatibility. J Biomed Mater Res Part A 2011;99A:295–306.

24) Audisio C, Raimondo S, Nicolino S, Gambarotta G, Di Scipio F, Macrì L, et al. Morphological and biomolecular characterization of the neonatal olfactory bulb ensheathing cell line. J Neurosci Methods 2009;185(1):89–98.

25) Wang J. Glass viscosity and structural relaxation by parallel plate rheometry, using a thermo-mechanical analyser. Mater Lett 1997;3(1):99–103.

26) Ahmed M, Earl DA. Characterizing glaze-melting behavior via HSM. Am Ceram Soc Bull 2002;81(3):47–52.

27) Martin SW, Angell CA. On the glass transition and viscosity of P_2O_5. J Phys Chem 1986;90(25):6736–40.

28) Geyling FT. Basic fluid-dynamic considerations in the drawing of optical fibers. At&T Tech J 1976;55:1011–56.

29) Paek UC, Runk RB. Physical behavior of the neck-down region during furnace drawing of silica fibers. J Appl Phys 1978;49(8):4417–22.

30) Goodman MN, Silver J, Jacobberger JW. Establishment and neurite outgrowth properties of neonatal and adult rat olfactory bulb glial cell lines. Brain Res 1993;619(1–2):199–213.

31) Mahay D, Terenghi G. Shawcross SG, Schwann cell mediated trophic effects by differentiated mesenchymal stem cells. Exp Cell Res 2008;314(14): 2692–701.

32) Fueshko S, Wray S. LHRH cells migrate on peripherin fibers in embryonic olfactory explant cultures: an in vitro model for neurophilic neuronal migration. Dev Biol 1994;166(1):331–48.

33) Shaim A, Et-tabirou M. Role of titanium in sodium titanophosphate glasses and a model of structural units. Mater Chem Phys 2003;80:63–7.

34) Brauer DS, Karpukhina N, Law RV, Hill RG. Effect of TiO_2 addition on structure, solubility and crystallisation of phosphate invert glasses for biomedical applications. J Non-Cryst Solids 2010;356(44–49):2626–33.

35) Navarro M, Ginebra MP, Clement J, Martinez S, Avila G, Planell JA. Physicochemical degradation of titania-stabilized soluble phosphate glasses for medical applications. J Am Ceram Soc 2003;86(8):1345–52.

36) Abou Neel EA, Chrzanowski W, Knowles JC. Effect of increasing titanium dioxide content on bulk and surface properties of phosphate-based glasses. Acta Biomater 2008;4:523–34.

37) Abou Neel EA, Chrzanowski W, Valappil SP, O'Dell LA, Pickup DM, Smith ME, Newport RJ, Knowles JC. Doping of a high calcium oxide metaphosphate glass with titanium dioxide. J Non-Cryst Solids 2009;355:991–1000.

38) Choueka J, Charvet JL, Alexander H, Oh YH, Joseph G, Blumenthal NC, et al. Effect of annealing temperature on the degradation of reinforcing fibers for absorbable implants. J Biomed Mater Res 1995;29(11):1309–15.

39) Cozien-Cazuc S, Parsons AJ, Walker GS, Jones IA, Rudd CD. Real-time dissolution of $P_{40}Na_{20}Ca_{16}Mg_{24}$ phosphate glass fibers. J Non-Cryst Solids 2009;355:2514–21.

40) Cozien-Cazuc S, Parsons AJ, Walker GS, Jones IA, Rudd CD. Effects of aqueous aging on the mechanical properties of P40Na20Ca16Mg24 phosphate glass fibres. J Mater Sci 2008;43:4834–9.

41) Stockhorst H, Brückner R. Deviations of structure between bulk and fiber glasses. J Phys Paris 1982;12(43)C9:451–454.

42) Abou Neel EA, Young AM, Nazhat SN, Knowles JC. A facile synthesis route to prepare microtubes from phosphate glass fibres. Adv Mater 2007;19(19):2856–62.

43) Rinehart JD, Taylor TD, Tian Y, Latour RA. Real-time dissolution measurement of sized and unsized calcium phosphate glass fibers. J Biomed Mater Res 1999;48(6):833–40.

44) Roacha P, Parker T, Gadegaard N, Alexander MR. Surface strategies for control of neuronal cell adhesion: a review. Surf Sci Rep 2010;65:145–73.

45) Geuna S, Raimondo S, Nicolino S, Boux E, Fornaro M, Tos P, et al. Schwann-cell proliferation in muscle–vein combined conduits for bridging rat sciatic nerve defects. J Reconstr Microsurg 2003;19(2):119–23.

46) Raimondo S, Nicolino S, Tos P, Battiston B, Giacobini-Robecchi MG, Perroteau I, et al. Schwann cell behavior after nerve repair by means of tissue-engineered muscle–vein combined guides. J Comp Neurol 2005;489(2):249–59.

47) Subramanian A, Krishnan UM, Sethuraman S. Development of biomaterial scaffold for nerve tissue engineering: biomaterial mediated neural regeneration. J Biomed Sci 2009;16(1):108–18.

48) Pigino G, Kirkpatrick LL, Brady ST. The cytoskeleton of neurons and glia. In: Siegel GJ, Albers RW, Brady S, Price D, editors. Basic neurochemistry: molecular, cellular, and medical aspects, Vol. 1.

49) Smeal RM, Rabbitt R, Biran R, Tresco PA. Substrate curvature influences the direction of nerve outgrowth. Ann Biomed Eng 2005;33(3):376–82.

50) Kim YT, Haftel VK, Kumar S, Bellamkonda RV. The role of aligned polymer fiberbased constructs in the bridging of long peripheral nerve gaps. Biomaterials 2008;29:3117–27.